NJC

Accepted Manuscript

This is an *Accepted Manuscript*, which has been through the Royal Society of Chemistry peer review process and has been accepted for publication.

Accepted Manuscripts are published online shortly after acceptance, before technical editing, formatting and proof reading. Using this free service, authors can make their results available to the community, in citable form, before we publish the edited article. We will replace this *Accepted Manuscript* with the edited and formatted *Advance Article* as soon as it is available.

You can find more information about *Accepted Manuscripts* in the Information for Authors.

Please note that technical editing may introduce minor changes to the text and/or graphics, which may alter content. The journal's standard Terms & Conditions and the Ethical guidelines still apply. In no event shall the Royal Society of Chemistry be held responsible for any errors or omissions in this *Accepted Manuscript* or any consequences arising from the use of any information it contains.

ROYAL SOCIETY OF CHEMISTRY

www.rsc.org/njc

The Synthesis of Shape-Controlled α-MoO_3 /Graphene Nanocomposites for High Performance Supercapacitors

Jinhua Zhou,[a1] Juan Song, [a1] Huihua Li, [1] Xiaomiao Feng,*[1] Zhendong Huang, [1] Shufen Chen, [1] Yanwen Ma,* [1] Lianhui Wang, [1] and Xiaohong Yan[2]

[1] Key Laboratory for Organic Electronics and Information Displays & Institute of Advanced Materials, National Jiangsu Syngerstic Innovation Center for Advanced Materials (SICAM);

[2] College of Electronic Science and Engineering,

Nanjing University of Posts & Telecommunications, 9 Wenyuan Road, Nanjing 210023, China

* Corresponding authors.

E-mail addresses: iamxmfeng@njupt.edu.cn, iamywma@njupt.edu.cn

[a] These authors contributed equally to this work.

Abstract: Novel nanoflake-like and nanobelt-like α-MoO_3/graphene nanocomposites were synthesized by a facile hydrothermal method through tailoring the content of Mo source, respectively. The formation mechanisms of α-MoO_3/graphene nanocomposites with different morphologies had been investigated. As a model, the α-MoO_3/graphene nanocomposites were studied for electrochemical energy storage supercapacitor devices. The results showed that α-MoO_3 nanoflakes/graphene occupied better supercapacitive performances than that of α-MoO_3 nanobelts/graphene, arising from the structural superiority and optimum compositions. It exhibited a high specific capacitance (up to 360 $F \cdot g^{-1}$) at a current density of 0.2 $A \cdot g^{-1}$, good rate capability, and a nearly 100% long-term cycle stability. This study provided a facile and optimal experimental design to gain α-MoO_3 /graphene composite materials act as a promising electrode material for high-performance supercapacitors.

1. Introduction

With the rapid development of the global economy and the growing of energy consumption, sustainable and clean energy sources are increasingly becoming societal trends nowadays, which greatly influence world economy and environment. The most promising energy storage systems should combine the features of relatively high energy density, good power capability, environmentally friendly, and low cost. [1]Among various energy storage devices, electrochemical capacitors (ECs), also known as supercapacitors or ultracapacitors, have attracted huge attention because of the high

New Journal of Chemistry Accepted Manuscript

power density and cycling stability,[2, 3] delivering much higher power densities than conventional batteries and higher energy densities than traditional capacitors.[4]

Among various influences, the performance of ECs is essentially determined by the electrode materials. Graphene, a two-dimensional nanosheet of graphite, has aroused growing attention as electrode materials. due to its outstanding electrical conductivity, excellent electrical mechanical properties, chemical stability, and high specific surface area up to 2675 $m^2 \cdot g^{-1}$.[5] Meanwhile, conductive polymers and metal oxides were also studied as electrode materials of pseudocapacitors,[6, 7] for which were endowed higher capacitance but experienced restricted lifetime and power densities because of phase changes during the redox process.[8]

Recently, graphene-based transition metal oxides composites as electrode materials of ECs have been studied widely for which can effectively overcome the low conductivity and cycling stability of metal oxides and the low capacitance of graphene.[9] For example, MnO_2/graphene,[10] Fe_3O_4/graphene,[11] NiO/graphene,[12] Co_3O_4/graphene,[13] TiO_2/graphene,[14] ZnO/graphene[15], and MoO_3/graphene[15] as most studied ECs electrode materials have shown excellent capacitive performances. Among these candicates, molybdenum trioxide (MoO_3) has attracted considerable attention as a promising supercapacitive material because of its low cost, nontoxicity, high electrochemical activity, and more environmentally benign nature than other transition-metal oxides.[16] MoO_3 is one kind of well-known transition metal oxide with the rich polymorphism, structural flexibility, and very stable two-dimensional (2D) layered structure. There are three basic polytypes of MoO_3 containing orthorhombic MoO_3 (α-MoO_3), monoclinic MoO_3 (β-MoO_3), and hexagonal MoO_3 (h-MoO_3), in which α-MoO_3 is the thermodynamically stable phase with layer structure.[17] α-MoO_3 has been intensively investigated and widely used in many fields including catalysts, biosensors, and energy storage due to its structural anisotropy. Mahmood et al. reported MoO_3 nanodots deposited on multiwalled carbon nanotubes with a specific capacitance of 91 $F \cdot g^{-1}$ at 0.4 $A \cdot g^{-1}$.[18] X. Zhang et al. prepared a Branchlike α-MoO_3/polypyrrole hybrid showing a specific capacitance of 129 $F \cdot g^{-1}$ at 5 $mV \cdot s^{-1}$.[16] α-MoO_3-decorated graphene sheets was synthesized by virtue of electrochemical

New Journal of Chemistry Accepted Manuscript

exfoliation, delivering a specific capacitance of 86.3 $F \cdot g^{-1}$ at 100 $mV \cdot s^{-1}$.[19]

In this report, nanoflake-like and nanobelt-like α-MoO_3/graphene composites were synthesized by a facile hydrothermal method through tailoring the content of the Mo source, respectively. Graphene acted as conductive and supporting materials for α-MoO_3. SEM and TEM results displayed the morphology of the α-MoO_3 varied from nanoflakes to nanobelts by increasing the content of Mo sources. XPS, FT-IR, and TGA were also used to investigate the structure and composition of the composites. The electrochemical properties of as-prepared α-MoO_3/graphene composites had been investigated. As a result, the nanoflake-like α-MoO_3/graphene showed better supercapacitive performance than that of nanobelt-like α-MoO_3/graphene, displaying a specific capacitance as high as 380 $F \cdot g^{-1}$ at a current density of 0.2 $A \cdot g^{-1}$, high rate discharge, and excellent long-term cycle stability approaching 100% in 1 M H_2SO_4.

2. Experimental

2.1 Chemicals

Natural graphite flake (about 325 mesh) was purchased from Alfa Aesar Chemical Reagent Co. Hexaammonium molybdate tetrahydrate ($(NH_4)_6Mo_7O_{24} \cdot 4H_2O$) was purchased from Sinopharm Chemical Reagent Co.,Ltd. HNO_3(68%) was obtained from Shanghai Ling Feng Chemical Reagent co., Ltd. Cetyltrimethyl ammonium bromide (CTAB) and poly(diallyldimethylammonium chloride) (PDDA, MW = 200 000–350 000) were purchased from Aladdin Reagent (Shanghai) co., Ltd. All reagents were analytical grade and used as received without further purification.

2.2 Preparation of different morphologies MoO_3/graphene composites

Graphene oxide (GO) suspension was prepared through the modified Hummer's method from natural flake graphite powder according the described process previously[20]. 100 mg GO powder was dissolved in 20 mL DI water under stirring. 100 μL PDDA was dropped into the obtained GO homogeneous dispersion and stirred for 30 minutes. 250 mg $(NH_4)_6Mo_7O_{24} \cdot 4H_2O$ and 50 mg CTAB were added to the above solution and kept stirring for one hour. 15 mL HNO_3 (68%) was dropped into the mixed solution to adjust pH value and stirred for 30 minutes. The resulted mixture was

New Journal of Chemistry Accepted Manuscript

removed into a Teflon-Lined autoclave with a stainless-steel shell and then maintained at 120 °C for 12 h. The final precipitate was collected and washed thoroughly with DI water and ethanol several times and then dried at 60 °C for 12 h. For contrast, the contents of $(NH_4)_6Mo_7O_{24}\cdot 4H_2O$ and CTAB were doubled, tripled, and quadrupled of the initial amount and other experimental conditions were unchanged, respectively. The final corresponding composites were named as MG-F-1, MG-F-2, MG-B-3 and MG-B-4 according to the structures of the composites and the content of Mo sources. Graphene and pure MoO_3 were gained respectively under the same conditions.

2.3 Characterization

The morphologies of composites were characterized by scanning electron microscopy (SEM, S-4800) and transmission electron microscope (TEM, JEOL-JEM-2100F at 100 kV). The structure of the composites was investigated by means of X-ray diffraction patterns (XRD, Bruker D8 Advance X-ray diffractometer). The composition of the products was examined by Fourier transform infrared spectroscopy (FT-IR, a Bruker model VECTOR-22 Fourier transform spectrometer). The X-ray photoelectron spectroscopic analysis was obtained using ESCALAB MK II X-ray photoelectron spectrometer. The thermogravimetry analysis (TGA) measurements were carried out with a DTG-60 thermal analyzer. Electrochemical experiments were investigated by a CHI660C electrochemical workstation (Chenhua, Shanghai). The three-electrode cell consisted of a platinum wire as counter electrode and saturated calomel electrode (SCE) as reference electrode, respectively. The working electrode was prepared by mixing active material, acetylene black, and polyfluortetraethylene (PTFE) at a weight ratio of 70: 25: 5 and pasted onto graphite electrode. The average loading amounts of active materials on the electrodes were 10 mg. The specific capacitance could be calculated from the cyclic voltammograms (CV) curves according to eqn 1:[21]

$$C_g = (\int IdV) \Big/ (mV\upsilon) \qquad (1)$$

Where I is the response current, V is the potential range, υ is the scan rate, and m is the mass of the active material in the electrode. The specific capacitance was calculated from the galvanostatic charge/discharge curves using eqn 2:[22]

$$C_g = I\Delta t / m\Delta V \qquad (2)$$

New Journal of Chemistry Accepted Manuscript

Where I represent the discharge current (A), Δt is the discharge time (s), m is the mass of the active material in the electrode, and ΔV is the potential window.

3. Results and discussion

3.1 Formation mechanism

Nanoflake-like and nanobelt-like α-MoO_3/graphene were synthesized by one-step hydrothermal method through changing the content of Mo sources, respectively. GO was highly negatively charged due to the presence of a large amounts of oxygen-containing functional groups on the surface and edges of GO nanosheets.[23] It has been positively charged after functionalized by PDDA, a linear positively charged polyelectrolyte,[24, 25] and can be bonded with negative $Mo_7O_{24}^{6-}$ by electrostatic interaction. H_2MoO_4 was firstly formed on the surface and edges of GO sheets under acidic condition caused by the addition of nitric acid. GO with large area provided plenty of attachment sites for the attachment of H_2MoO_4 nucleus. During hydrothermal process, H_2MoO_4 gradually decomposed into α-MoO_3 on the surface of GO and GO were reduced to graphene. With the increasing content of $(NH_4)_6Mo_7O_{24}\cdot 4H_2O$, the corresponding α-$MoO_3$ achieved the morphlolgy change from nanoflakes to nanobelts. At low concentration of $Mo_7O_{24}^{6-}$, the generation rate of H_2MoO_4 nucleus was slow with small nucleation rate and then agglomerated by physical absorption while CTAB worked as soft template. The adsorption of on graphene could occur in two dimension and then growed in two directions to form nanoflake.[26] With graphene acting as a substrate, α-MoO_3 nanoflakes lied down along the substrate with their large surfaces parallel to the substrate.[27] It is a common phenomenon in the synthesis of inorganic nanomaterials that high supersaturation will curb the growth of preformed nuclei in two dimension and lead to the formation of hierarchical structures.[28] While adding into more $(NH_4)_6Mo_7O_{24}$ to increase concentration of $Mo_7O_{24}^{6-}$, the generating crystal nucleus speed was great and the diffusion of $Mo_7O_{24}^{6-}$ might be obstructed. The post growth of those existing nucleus would be hindered. More CTAB resulted in the concentration of CTAB exceeding critical micelle concentration, which decreasing the efficiency of template. As a result, α-MoO_3 nanobelts were the final prouducts.

New Journal of Chemistry Accepted Manuscript

3.2 Morphologies and composition characterization

The morphology and microstructure of the obtained α-MoO_3/graphene composites were characterized by TEM and SEM under different magnifications. Fig. 1A and Fig. 1B showed the SEM and TEM images of pure graphene, in which graphene appeared transparent and thin platelet with curled and wavy wrinkle. Fig. 1C displayed the SEM image of MG-F-1 that graphene platelets were decorated by α-MoO_3 to form the composite nanoflakes. Compared with pure graphene, the thickness of the graphene platelets decorated by α-MoO_3 increased. And graphene platelet lost the transparent wrinkle, which could be further confirmed by the TEM image. With the doubled content of $(NH_4)_6Mo_7O_{24}\cdot 4H_2O$, the corresponding TEM images of the composite nanoflakes became darker and their thickness was enhanced than that of MG-F-1, as shown in Fig. 1C and 1D. For the above two composites, α-MoO_3 completely deposited on graphene platelets and the structure was loose caused by electrostatic repulsion among the negatively charged graphene platelets with the residual oxygen-containing functional groups. Fig. 1G revealed SEM image of MG-B-4 with many α-MoO_3 nanobelts adsorbed on the surface of the graphene. The TEM images of MG-B-4 (Fig. 1H) revealed that many α-MoO_3 nanobelts were anchored on the thin graphene layers and α-MoO_3 nanobelts showed an average diameter of around 200 nm and lengths between 1 and 2 μm.

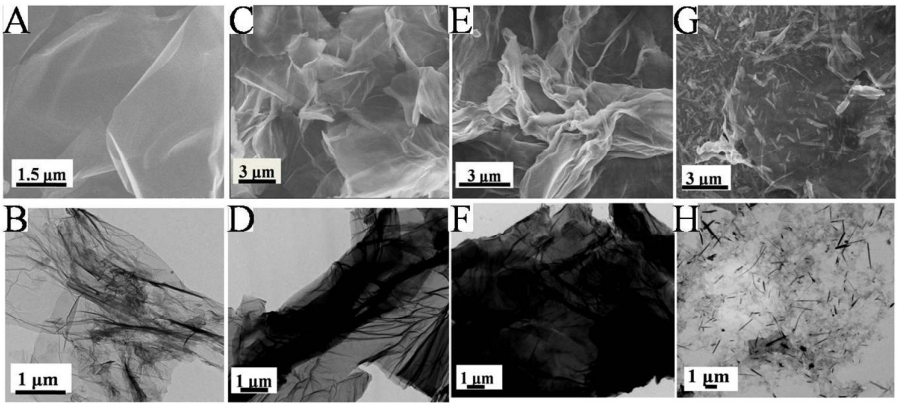

Fig. 1. SEM (A, C, E, and G) and TEM (B, D, F, and H) images of graphene (A/B), MG-F-1 (C/D), MG-F-2 (E/F), and MG-B-4 (G/H)

Fig. 2 showed the XRD patterns of GO and α-MoO_3/graphene composites. GO

New Journal of Chemistry Accepted Manuscript

showed a strong diffraction peak at around 10.7° corresponding to the (001) reflection of the stacked GO platelets.[29] After combination, the diffraction peaks positioned at 12.7, 23.1, 25.4, 27.0, 33.4, 38.8, 45.6, 49.2, 55.0, and 58.9° were in good agreement with the standard peaks for the orthorhombic phase of α-MoO_3 (α-MoO_3, JCPDS card No. 05-0508)[30] and no diffraction peaks from GO were observed, indicating that the surfaces of graphene were fully decorated by α-MoO_3. The diffraction peak intensity of α-MoO_3 became stronger from MG-F-1 to MG-B resulting from the increased content of α-MoO_3. In addition, the intensities of the (020), (040) and (060) peaks were stronger which indicated the anisotropic growth of the nanostructure, as well as the preferred orientation of the layered structure α-MoO_3.[27, 31]

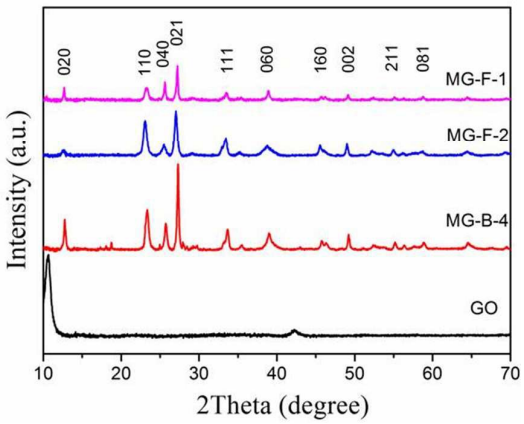

Fig. 2. XRD patterns of GO, MG-F-1, MG-F-2, and MG-B-4

The FT-IR spectra of GO, MG-F-1, MG-F-2, and MG-B-4 were shown in Fig. 3. The spectrum of the oxygen-containing functional groups of GO revealed the bands at 1070, 1227, 1397, and 1739 cm^{-1}, which corresponded to the stretching vibrations of alkoxy C–O, epoxy C-O, carboxy C-OH, and C=O groups from carbonyl and carboxylic groups respectively. Moreover, absorption at 3440 cm^{-1} and 1617 cm^{-1} could be attributed to O-H stretching vibrations and bending vibrations of adsorbed water molecules or structural O-H groups.[32] However, the peaks of oxygen-containing functional groups in the composites became weakened, indicating part of the surface oxygen-containing functional groups had been deoxygenized during hydrothermal process. For the spectra of the composites, three typical peaks at 995, 862, and 568

New Journal of Chemistry Accepted Manuscript

cm^{-1} were the characteristic of the peaks of α-MoO_3. The peak at 995 cm^{-1} was due to the terminal Mo=O bond, layered orthorhombic α-MoO_3 phase.[33] The band at 862 cm^{-1} was assigned to the doubly coordinated oxygen (Mo_2–O) stretching mode which results from the corner-shared oxygen in common with two MoO_6 octahedra, and the band at 568 cm^{-1} belonged to the bending vibration of the Mo–O–Mo entity, while the O ion was shared by three Mo ions.[19]

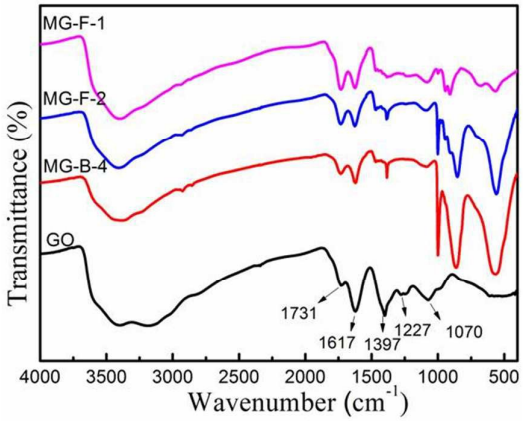

Fig. 3. FTIR spectra of GO, MG-F-1, MG-F-2, and MG-B-4

The surface chemistry of the composites was analyzed by XPS. The wide scan XPS (Fig. 4a) showed that the spectra of MG-F-1 and MG-B-4 composites contained a new Mo element compared to the spectrum of GO, demonstrating the success combination of MoO_3 with graphene. Fig. 4b exhibited the C1s XPS spectra of GO, MG-F-1, and MG-B-4, which could be divided four Gaussian peaks centered at 284.6, 286.8, 288.5, and 289.3 eV assigned to C-C/C=C, C-O, C=O, and O=C-O groups, respectively. Notably, the three Gaussians peaks for oxygen-containing functional groups became weak in the curves of MG-F-1 and MG-B, which indicated most oxygen-containing groups had been removed through hydrothermal process. In the spectrum of Mo 3d (Fig. 4c), the peaks of Mo3d5/2 and Mo3d3/2 were located at 232.1 and 235.3 eV with an integrated peak area ratio of 3:2 and binding energy (ΔMo 3d=3.1eV), corresponding to Mo(VI) for α-MoO_3.[34]

New Journal of Chemistry Accepted Manuscript

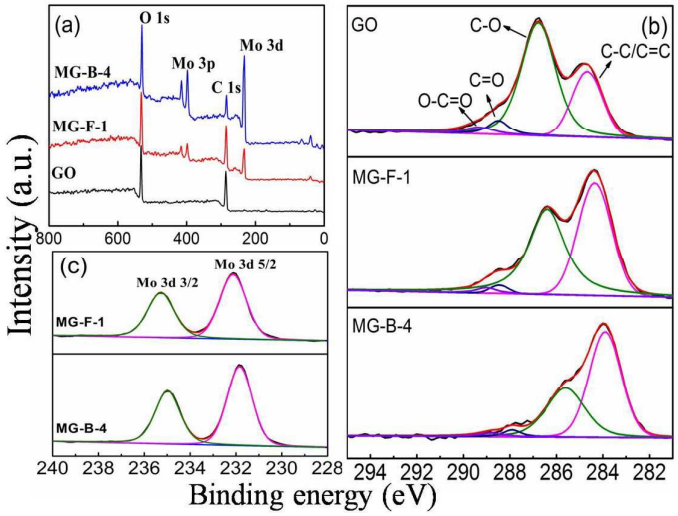

Fig. 4. XPS spectra (a) survey scan of GO, MG-F-1, and MG-B, (b) C1s of GO, MG-F-1, and MG-B-4, (c) Mo 3d of MG-F-1 and MG-B-4.

Thermal stability of α-MoO_3/graphene composites were investigated by TGA, which were performed with a heating rate of 10 °C·min^{-1} in air atmosphere. The mass loss below 230 °C could be attributed to the evaporation of adsorbed water and decomposition of the labile oxygen-containing functional groups.[35] An obvious mass loss appeared between 230 and 530 °C, owing to the pyrolysis of some residual surfactant and complete oxidation of graphene to carbon dioxide in air atmosphere. Then the curves kept thermal stability plateaus from 530 °C until 730 °C followed by an obvious mass loss of the nanocomposites belonged to the melting and then evaporating behavior process of α-MoO_3 after 730 °C.[27] After the thermal stability plateaus, graphene was oxidized to carbon dioxide and the residual wt.-% referred to the weight percentage content α-MoO_3 of in the composites. The mass percent of α-MoO_3 in the composites were 19.6%, 60.1%, and 83.5% corresponding to MG-F-1, MG-F-2, and MG-B-4, respectively.

New Journal of Chemistry Accepted Manuscript

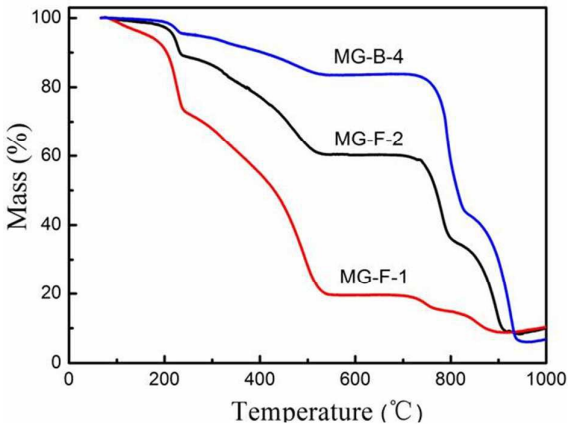

Fig. 5. TGA curves of MG-F-1, MG-F-2, and MG-B-4.

3.3 Electrochemical characterization

The cyclic voltammogram (CV) and galvanostatic charge/discharge (GCD) measurements were carried out to study the electrochemical properties of MG-F-1, MG-F-2 and MG-B-4. Fig. 6a showed the CV curves of MG-F-1, MG-F-2, and MG-B-4 at a scan rate of 100 $mV \cdot s^{-1}$ with potential windows between 0 and 1.0 V. Obviously, MG-F-2 showed largest enclosed area of the CV curve among the three samples, implying MG-F-2 possessed best capacitive performance. According to eqn 1, the calculated specific capacitance of MG-F-1, MG-F-2, and MG-B-4 were 82.1, 119.8, and 96.0 $F \cdot g^{-1}$, respectively. In the Fig. 6b, the GCD curves at a current density of 1 $A \cdot g^{-1}$ indicated the corresponding discharge time and MG-F-2 possessed the longest discharge time among of MG-F-1, MG-F-2, and MG-B-4, illustrating MG-F-2 had highest capacitance values. The calculated specific capacitance based on eqn 2 of MG-F-1, MG-F-2, and MG-B-4 were 132.0, 209.0, and 152.1 $F \cdot g^{-1}$, respectively. For the composites, α-MoO_3 generated pseudocapacitance by the reaction between H^+ cations and α-MoO_3 resulting in a partial reduction of Mo^{6+} to Mo^{5+}, while graphene effectively created conducting paths for the electrons and generated EDLC, thus improving the overall capacitance of the composite electrodes. The main reasons for the excellent capacitance performance of MG-F-2 could be described as follow: Firstly, nanoflake-like α-MoO_3/graphene exhibited high contact areas with electrolyte ion, which was beneficial to improve the specific capacitance by shortening the diffusion and migration length of the electrolyte ions. Nanoflake-like α-MoO_3/graphene were

New Journal of Chemistry Accepted Manuscript

considered structurally superior to nanobelt-like α-MoO_3/graphene. Secondly, the IR drop of the composites were 0.044, 0.041, and 0.022 V for MG-F-1, MG-B-4, and MG-F-2 from the discharge curves at 1 $A \cdot g^{-1}$, the corresponding impedance of each voltage drop were 4.4, 4.1, and 2.2 Ω respectively, which elucidated MG-F-2 possessed preferable electrical conductivity. Lastly, the pseudocapacitance and EDLC should be balanced in the composite electrodes to achieve the optimum capacitive behavior.[4] Comparison to MG-F-1, an appropriate higher loading of α-MoO_3 in MG-F-2 according to the TG results enhanced the overall capacitance by virtue of improving the pseudocapacitance. The highest content of α-MoO_3 was observed in MG-B-4 but the presence of excess α-MoO_3 in the composites could be a burden for optimum compositions that exhibited by MG-F-2.[34]

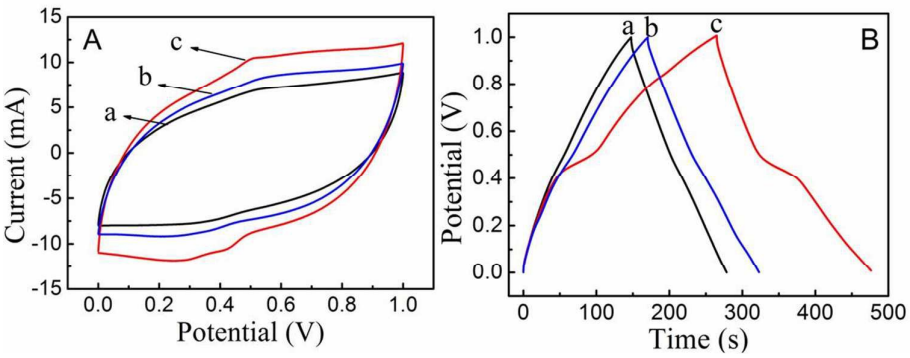

Fig. 6. CV curves of MG-F-1(a), MG-B-4 (b), and MG-F-2 (c) at a scan rate of 100 $mV \cdot s^{-1}$ (A), GCD curves of MG-F-1(a), MG-B-4 (b), and MG-F-2 (c) at a current density of 1 $A \cdot g^{-1}$ (B)

The electrochemical behavior and capacitive performance of MG-F-2 were evaluated by CV and GCD measurements as shown in Fig. 7. The CV curves of MG-F-2 were investigated in the potential window of 0-1.0 V at scan rates of 2, 5, 10, 25, 50, 75, and 100 $mV \cdot s^{-1}$ in 1M H_2SO_4 aqueous solution (Fig. 7a). A pair of redox peaks illustrated the redox activity of α-MoO_3 in 1 M H_2SO_4 and the redox reaction shown in eqn 3.

$$2Mo^{VI}O_3 + 2H^+ + 2e^- \rightarrow Mo^{V}{}_2O_5 + H_2O \quad (3)[31]$$

At low scan rates, pseudocapacitance played the main role while more active α-MoO_3 were sufficiently introduced into the above redox reaction. With the increasing scan

New Journal of Chemistry Accepted Manuscript

rates, the rectangle-shaped and symmetric shape CV curves were distorted because of the double-layer and pseudocapacitive contributions to the total capacitance. The calculated specific capacitance values of MG-F-2 at 2, 5, 10, 25, 50, 75, and 100 $mV \cdot s^{-1}$ were 265.0, 184.3, 171.0, 155.1, 139.6, 128.4, and 119.8 $F \cdot g^{-1}$, respectively (Fig. 7b). Fig. 7c showed the GCD curves of MG-F-2 at different current densities. The curves showed a nonlinear charge–discharge curve, indicating that the material had pseudocapacitive behavior and were nearly symmetrical, which was another typical characteristic of an ideal supercapacitor. No obvious IR drop in the discharge curves was observed due to good electrical properties of graphene. The calculated specific capacitances of MG-2 are 361.0, 275.8, 239.2, 217.6, 209.0, 158.0, and 148.2 $F \cdot g^{-1}$ at 0.2, 0.4, 0.6, 0.8, 1.0, 2.0, and 3.0 $A \cdot g^{-1}$, respectively. The specific capacitance was reduced with the increase of current densities but it was still kept 148.2 $F \cdot g^{-1}$ when current density increased to 3.0 $A \cdot g^{-1}$. On one hand, reaction of H^+ cations with electroactive material following by a redox reaction gained the charge storage occurring in the layered structure of α-MoO_3, strongly enhanced the capacitive performance. On the other hand, the graphene in composite played an important role for improving the capacitive property, which was intertwined and intimately bonded with α-MoO_3, serving dual functions as both conductive channels and active interface centers and offered better interconnectivity between α-MoO_3 and further more participates in electrochemical double layer capacitance.[36]

New Journal of Chemistry Accepted Manuscript

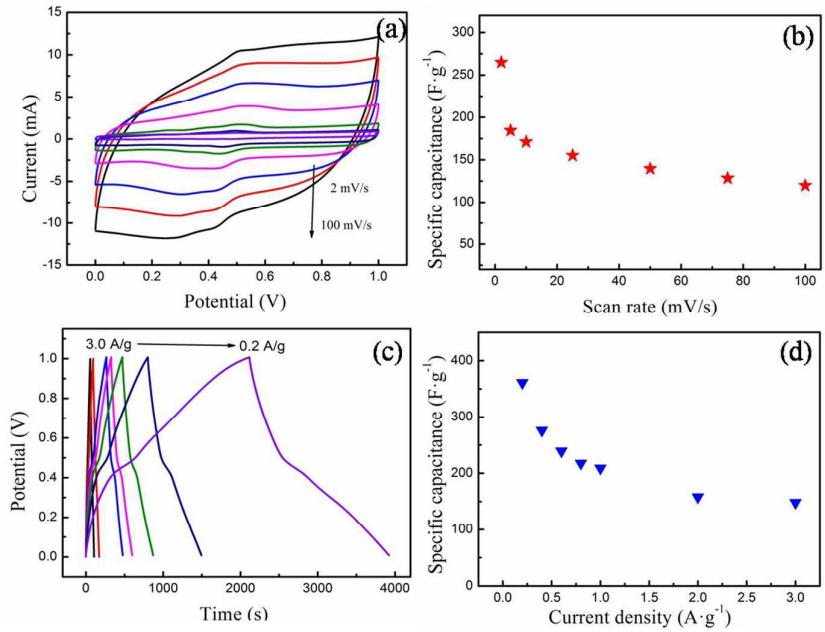

Fig. 7. CV curves of MG-F-2 at different scan rates: from inner to outside (2, 5, 10, 25, 50, 75, and 100 $mV \cdot s^{-1}$) (a) and the corresponding specific capacitance of MG-F-2 at different scan rates (b). GCD curves of MG-F-2 at different current densities: from left to right (3.0, 2.0, 1.0, 0.8, 0.6, 0.4, 0.2 $A \cdot g^{-1}$) (c) and the corresponding specific capacitance of MG-F-2 at different current densities (d)

The cycle stability was another important parameter for supercapacitors. The cycle stability of MG-F-2 was determined by galvanostatic charge/discharge tested at a current density of 1.0 $A \cdot g^{-1}$ for 1000 cycles. With the increasing cycles, the specific capacitance of MG-F-2 showed almost no loss, nearly 100% retention after 1000 cycles, which was assigned to the excellent stable structure and the synergistic effect between α-MoO_3 and graphene. The nanoflake-like α-MoO_3/graphene with stable layered structure α-MoO_3 attached on graphene nanoplates tightly through Mo atom binding with the oxygen containing function groups and could keep fine with less degradation during charge/discharge processes. During the redox reaction of H^+ cations with electroactive material, the H^+ cations were faradaically stored in the layered structure and prohibit the phase transition (structural rearrangement). In addition, the mechanical stability of graphene in the MG-F-2 composite could keep long term cycle stability of the composite because of EDLCs proved higher stability than pseudocapacitance .[37]

New Journal of Chemistry Accepted Manuscript

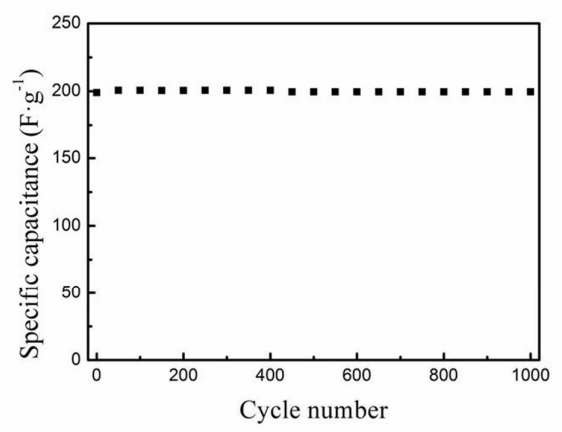

Fig. 8. The specific capacitance changes of MG-F-2 at a constant current density of 1 $A \cdot g^{-1}$ as a function of cycle numbers

4. Conclusions

α-MoO_3/graphene composites were successfully synthesized by one step hydrothermal method. The morphology of the α-MoO_3 in the composites varied from nanoflakes to nanobelts by increasing the content of Mo sources. The α-MoO_3 /graphene composites exhibited outstanding supercapacitive properties acting as the electrode materials. Among all the samples, MG-F-2 delivered the best excellent capacitive performances with a specific capacitive of 360 $F \cdot g^{-1}$ arising from the structural superiority and optimum compositions than other composites. Besides, MG-F-2 revealed exellent long term cycling stability, approaching 100%. This research offers the rational design strategy of advanced electrode materials of supercapaitors on a basis of combination of α-MoO_3 and graphene with the well-defined nanostructures for future applications in energy conversion and storage.

Acknowledgments.

We sincerely express our thanks to the '973' (2012CB933301) and '863' projects (2011AA050526), the National Natural Science Foundation of China (Nos. 20905038, 20903057, and 61274065), and the Natural Science Foundation of Jiangsu (BK20141424), and the Program of Nanjing University of Posts and Telecommunications (NY214088), and the Open Research Fund of State Key Laboratory of Bioelectronics (I2015010), Southeast University, and the Priority Academic Program Development of Jiangsu Higher Education Institutions (PAPD), and the Ministry of Education of China (IRT1148).

References

New Journal of Chemistry Accepted Manuscript

1. P. J. Lu, M. Lei and J. Liu, *Cryst. Eng. Comm.*, 2014, **16**, 6745-6755.
2. H. Jiang, J. Ma and C. Z. Li, *Adv. Mater.*, 2012, **24**, 4197-4202.
3. B. G. Choi, M. Yang, W. H. Hong, J. Choi and Y. S. Huh, *ACS Nano*, 2012, **6**, 4020-4028.
4. S. D. Perera, A. D. Liyanage, N. Nijem, J. P. Ferraris, Y. J. Chabal and K. J. Balkus, *J. Power Sources*, 2013, **230**, 130-137.
5. B. Xu, S. F. Yue, Z. Y. Sui, X. T. Zhang, S. S. Hou, G. P. Cao and Y. S. Yang, *Energy Environ. Sci.*, 2011, **4**, 2826-2830.
6. Y. Huang, J. J. Liang and Y. S. Chen, *Small*, 2012, **8**, 1805-1834.
7. M. Epifani, T. Chávez-Capilla, T. Andreu, J. Arbiol, J. Palma, J. R. Morante and R. Díaz, *Energy Environ. Sci.*, 2012, **5**, 7555-7558.
8. J. Yang and L. Zou, *Electrochim. Acta*, 2014, **130,** 791-799.
9. C. H. Xu, B. H. Xu, Y. Gu, Z. G. Xiong, J. Sun and X. S. Zhao, *Energy Environ. Sci.*, 2013, **6**, 1388-1414.
10. Z. S. Wu, W. Ren, D. Wang, F. Li, B. Li and H. Cheng, *ACS Nano*, 2010, **4**, 5835-5842.
11. G. M. Zhou, D. W. Wang, F. Li, L. L. Zhang, N. Li, Z. S. Wu, L. Wen, G. Q. Lu and H. M. Cheng, *Chem. Mater.*, 2010, **22**, 5306-5313.
12. B. Zhao, J. S. Song, P. Liu, W. W. Xu, T. Fang, Z. Jiao, H. J. Zhang and Y. Jiang, *J. Mater. Chem.*, 2011, **21**, 18792-18798.
13. Z. S. Wu, W. C. Ren, L. Wen, L. B. Gao, J. P. Zhao, Z. P. Chen, G. M. Zhou, F. Li and H. M. Cheng, *ACS Nano*, 2010, **4**, 3187-3194
14. T. Lu, Y. P. Zhang, H. B. Li, L. K. Pan, Y. L. Li and Z. Sun, *Electrochim. Acta*, 2010, **55**, 4170-4173.
15. A. Ramadoss and S. J. Kim, *Mater. Chem. Phys.*, 2013, **140**, 405-411.
16. X. Zhang, X. Z. Zeng, M. Yang and Y. X. Qi, *ACS Appl. Mater. Inter.*, 2014, **6**, 1125-1130.
17. X. F. Yang, H. Y. Ding, D. Zhang, X. H. Yan, C. Y. Lu, J. L. Qin, R. X. Zhang, H. Tang and H. J. Song, *Cryst. Res. Technol.*, 2011, **46**, 1195-1201.
18. Q. Mahmood, H. J. Yun, W. S. Kim and H. S. Park, *J. Power Sources*, 2013,

New Journal of Chemistry Accepted Manuscript

235, 187-192.

19. J. B. Hu, A. Ramadan, F. Luo, B. Qi, X. J. Deng and J. Chen, *J. Mater. Chem.*, 2011, **21**, 15009-15014.
20. X. M. Feng, R. M. Li, Y. W. Ma, R. F. Chen, N. E. Shi, Q. L. Fan and W. Huang, *Adv. Funct. Mater.*, 2011, **21**, 2989-2996.
21. J. Zhu and J. He, *ACS Appl. Mater. Interf.*, 2012, **4**, 1770-1776.
22. L. F. Lai, H. P. Yang, L. Wang, B. K. Teh, J. Q. Zhong, H. Chou, L. W. Chen, W. Chen, Z. X. Shen, R. S. Ruoff and J. Y. Lin, *ACS Nano*, 2012, **6**, 5941-5951.
23. Z. S. Wu, W. Ren, D. W. Wang, F. Li, B. Liu and H. M. Cheng, *ACS Nano*, 2011, **4**, 5835-5842.
24. K. Liu, J. Zhang, G. Yang, C. Wang and J. J. Zhu, *Electrochem. Commun.*, 2010, **12,** 402-405.
25. Y. Z. Su, S. Li, D. Q. Wu, F. Zhang, H. W. Liang, P. F. Gao, C. Cheng and X. L. Feng, *ACS Nano*, 2012, **6**, 8349-8356.
26. X. Feng, Z. Yan, N. Chen, Y. Zhang, Y. Ma, X. Liu, Q. Fan, L. Wang and W. huang, *J. Mater. Chem. A*, 2013, **1**, 12818-12825.
27. D. L. Chen, M. N. Liu, L. Yin, T. Li, Z. Yang, X. J. Li, B. B. Fan, H. L. Wang, R. Zhang, Z. X. Li, H. L. Xu, H. X. Lu, D. Y. Yang, J. Sun and L. Gao, *J. Mater. Chem.*, 2011, **21**, 9332-9342
28. L. Xi and Y. M. Lam, *Chem. Mater.*, 2009, **21**, 3710-3718.
29. J. Yan, Q. Wang, T. Wei, L. L. Jiang, M. L. Zhang, X. Y. Jing and Z. J. Fan, *ACS Nano*, 2014, **5**, 4720-4729.
30. S. Balendhran, S. Walia, M. Alsaif, E. P. Nguyen, J. Z. Ou, S. Zhuiykov, S. Sriram, M. Bhaskarah and K. Kalantar-zadeh, *ACS Nano*, 2013, **11**, 9753-9760.
31. B. Mendoza-Sánchez, T. Brousse, C. Ramirez-Castro, V. Nicolosi and P. S.Grant, *Electrochim. Acta*, 2013, **91**, 253-260.
32. D. D. Cai, S. Q. Wang, L. X. Ding, P. C. Lian, S. Q. Zhang, F. Peng and H. H. Wang, *J. Power Source*, 2014, **254**, 198-203.
33. X. F. Xia, Q. L. Hao, W. Lei, W. J. Wang, H. L. Wang and X. Wang, *J. Mater. Chem.*, 2012, **22**, 8314-8320.

New Journal of Chemistry Accepted Manuscript

34. C. L. Liu, Y. Wang, C. Zhang, S. L. Xiao and W. S. Dong, *Mater. Chem. Phys.*, 2014, **143**, 1111-1118.

35. Y. W. Zhu, S. Mural, M. D. Stoller, A. Velamakanni, R. D. Piner and R. S. Ruoff, *Carbon*, 2010, **48**, 2106-2122.

36. J. Chang, M. H. Jin, F. Yao, T. H. Kim, V. T. Le, H. Y. Yue, F. Gunes, B. Li, A. Ghosh, S. S. Xie and Y. H. Lee, *Adv. Funct. Mater.*, 2013, **23**, 5074-5083.

37. J. W. Lee, A. S. Hall, J. D. Kim and T. E. Mallouk, *Chem. Mater.*, 2012, **24**, 1158-1164

New Journal of Chemistry Accepted Manuscript

Graphical Abstract

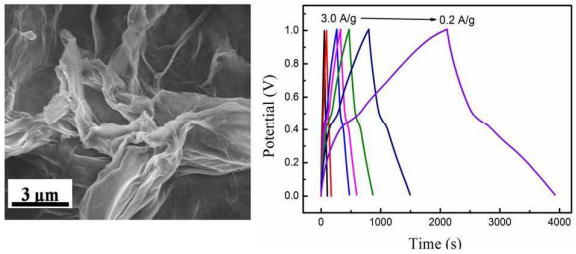

Novel nanoflake-like α-MoO_3/graphene nanocomposites were synthesized and exhibited a high specific capacitance up to 360 $F \cdot g^{-1}$ and excellent long term cycle stability.

New Journal of Chemistry Accepted Manuscript